Connectome of memristive nanowire networks through graph theory

Neural Networks 150 (2022) 137–148

Contents lists available at ScienceDirect

Neural Networks

journal homepage: www.elsevier.com/locate/neunet

Connectome of memristive nanowire networks through graph theory

Gianluca Milano [a,*], Enrique Miranda [b], Carlo Ricciardi [c,*]

[a] Advanced Materials Metrology and Life Sciences Division, INRiM (Istituto Nazionale di Ricerca Metrologica), Strada delle Cacce 91, 10135 Torino, Italy
[b] Departament d'Enginyeria Electrònica, Universitat Autònoma de Barcelona (UAB), 08193 Barcelona, Spain
[c] Department of Applied Science and Technology, Politecnico di Torino, C.so Duca degli Abruzzi 24, 10129 Torino, Italy

ARTICLE INFO

Article history:
Received 5 October 2021
Received in revised form 26 January 2022
Accepted 24 February 2022
Available online 7 March 2022

Dataset link: https://doi.org/10.5281/zenodo.6322736

Keywords:
Neuromorphic hardware
Neuromorphic nanowire networks
Self-organizing networks
Emergent dynamics
Memristive networks
Unconventional computing

ABSTRACT

Hardware implementation of neural networks represents a milestone for exploiting the advantages of neuromorphic-type data processing and for making use of the inherent parallelism associated with such structures. In this context, memristive devices with their analogue functionalities are called to be promising building blocks for the hardware realization of artificial neural networks. As an alternative to conventional crossbar architectures where memristive devices are organized with a top-down approach in a grid-like fashion, neuromorphic-type data processing and computing capabilities have been explored in networks realized according to the principle of self-organization similarity found in biological neural networks. Here, we explore structural and functional connectivity of self-organized memristive nanowire (NW) networks within the theoretical framework of graph theory. While graph metrics reveal the link of the graph theoretical approach with geometrical considerations, results show that the interplay between network structure and its capacity to transmit information is related to a phase transition process consistent with percolation theory. Also the concept of *memristive distance* is introduced to investigate activation patterns and the dynamic evolution of the information flow across the network represented as a *memristive graph*. In agreement with experimental results, the emergent short-term dynamics reveals the formation of self-selected pathways with enhanced transport characteristics connecting stimulated areas and regulating the trafficking of the information flow. The network capability to process spatio-temporal input signals can be exploited for the implementation of unconventional computing paradigms in memristive graphs that take into advantage the inherent relationship between structure and functionality as in biological systems.

1. Introduction

The human brain is a complex biological network where an emergent behavior arises from interactions of neurons mediated by synaptic connections. Connectome, as the comprehensive map of neural connections within the nervous system, represents the backbone of brain functionalities (Sporns, 2011; Sporns, Tononi, & Kötter, 2005). In this context, understanding the function of brain is inextricably related to mapping its elements and connections, creating a structural description of the 3D network architecture. This is the main goal of the connectionism, an approach developed in the cognitive science field that aims to describe cognitive phenomena by means of interconnected networks of simple parallel computing elements. This approach is related also to the development of artificial neural networks (ANNs) where learning occurs through distributed signal activity across the network where connection strengths (synaptic weights) are modified based on the experience, being this the basis of both neuroinformatics and neuromorphic computing. Indeed, the study of biological neural circuits has stimulated the development of computing paradigms based on ANNs and machine learning, also known as brain-inspired computing, paving the way for the development of artificial intelligence.

Recent trends in neuromorphic computing basically rely on mimicking brain functionalities and neural network architectures on hardware platforms, driving the development of new components able to emulate neurons and synapses at the individual level (Christensen et al., 2022; Tang et al., 2019; Upadhyay et al., 2019). Among these components, memristive devices organized in large-scale crossbar arrays to form neural networks have been demonstrated as promising platforms for brain-inspired computing paradigm taking into advantage the so-called in-memory computing (Xia & Yang, 2019). However, these neuromorphic systems have been realized by means of regular arrays of memristive elements, a hardware architecture that strongly differs from the intrinsic structural complexity of biological neural networks. With the aim of emulating the structure–function relationship of

* Corresponding authors.
E-mail addresses: g.milano@inrim.it (G. Milano), carlo.ricciardi@polito.it (C. Ricciardi).

https://doi.org/10.1016/j.neunet.2022.02.022

biological neural networks, biologically plausible neuromorphic architectures have been developed by self-organization with a bottom-up approach of memristive nano objects such as nanoparticles and nanowires to form memristive nanonetworks or atomic switch networks (Akai-Kasaya et al., 2022; Diaz-Alvarez, Higuchi, Li, Shingaya, & Nakayama, 2020; Diaz-Alvarez et al., 2019; Hochstetter et al., 2021; Li et al., 2020; Loeffler et al., 2020; Mallinson et al., 2019; Manning et al., 2018; Milano et al., 2020, 2021; Milano, Porro, Valov, & Ricciardi, 2019; Pantone, Kendall, & Nino, 2018; Pike et al., 2020; Scharnhorst et al., 2018; Shirai et al., 2020; Stieg et al., 2014; Tanaka et al., 2018; Zhu et al., 2021). As in the case of biological neural circuits, these neuromorphic architectures are complex systems where an emergent behavior arises from collective and group interaction phenomena. Their emergent dynamic behavior has been exploited for neuromorphic-type data processing (Hochstetter et al., 2021; Mallinson et al., 2019; Milano, Pedretti et al., 2020; Zhu et al., 2021) and for the implementation of novel computing paradigms (Lilak et al., 2021; Milano et al., 2021; Suarez, Kendall, & Nino, 2018; Usami et al., 2021). As occurs for all complex systems that pervade science, from the World-Wide Web to social networks and electrical power grids, understanding the network topology and connectivity is an essential requirement since the network structure ultimately determines its functions (Strogatz, 2001; Turnbull et al., 2018). Indeed, the structure–function relationship represents a fundamental principle of biological neuronal networks (Suárez, Markello, Betzel, & Misic, 2020; Suárez, Richards, Lajoie, & Misic, 2021).

In biological systems, complete reconstruction of a nervous system connectome from electron micrographs was achieved by considering the soil nematode *Caenorhabditis elegans* (Eichelmann, Oja, Eatherall, & a Walker, 1986; Witvliet et al., 2021). The reconstruction of the complete wiring diagram was in this case facilitated by the limited number of elements constituting the neural networks composed of about 300 neurons and 7000 synapses, a biological neural circuit much simpler than the human brain composed of about 10^{14}–10^{15} synaptic connections. While the map of the *C. elegans* nervous system represents the only complete connectome of a living organism, different methods have been employed to analyze the human brain connectivity at different scale levels, from microscale, where single neurons and synapses are analyzed, to the macroscale, by considering the interactions in between different brain regions (Sporns, 2011, 2018). Regardless of the spatial scale feature, biological neural networks are usually described as mathematical objects within the theoretical framework of graph theory linking neuroscience to network science (Vecchio, Miraglia, & Rossini, 2017). Despite the overwhelming potential in exploring the structure–function relationship of biological neural circuits of the brain, the power of network science and graph theory in analyzing hardware-implemented artificial neural network structure and its dynamics is still a rather unexplored field.

In this work, we investigate the structural and functional connectivity of self-organized memristive nanowire (NW) networks by means of a graph theory. The evolution of the interconnection topology as a function of the network density and NW length statistical distribution is investigated by means of graph metrics, showing that the results obtained with graph theory are in line with geometric considerations. Moreover, the consistency of the graph approach with percolation theory is reported, showing that the onset of percolation in NW networks is observed in correspondence with the emergence of a giant connected component in the graph induced by a progressive network density increase. The analysis of the giant connected component through graph metrics including the shortest path length, graph diameter, and average clustering coefficient suggests that the network exhibits small-world connectivity. The network functional connectivity of the memristive graph, where the emergent network dynamics rely on the mutual interaction of a large number of memristive NW junction edges, was investigated by introducing the concept of *memristive distance*. In agreement with experimental results, short-term memristive dynamics upon external stimulation of the network shows the emergence of a peculiar activation pattern, with formation of self-selected conductive pathways with enhanced information flow connecting stimulated network areas. The spatio-temporal dynamics of the NW networks can be exploited for implementation of graph-based unconventional computing paradigms in biologically inspired neuromorphic systems with direct relationship in between structure and function similarly to what happens in our brain.

2. Results and discussion

Memristive NW networks are realized by randomly dispersing memristive NWs on an insulating substrate, as reported in the SEM images shown in Fig. 1a, where memristive Ag NWs in suspension were drop-casted on an insulating substrate. The connectivity of the system is provided by the nanoscale cross-point junctions at the intersections of the NWs, as can be observed in Fig. 1b and c. While the metallic Ag NW core is highly conductive, each NW junction represents a memristive cell where the internal state of resistance (i.e. the synaptic weight) depends on the history of applied electrical stimuli. As a complex system, unraveling the link between structure and function of the neuromorphic NW network requires an analysis of its: *(i) structural connectivity* concerning the network architecture backbone represented by an undirected and unweighted graph; (ii) *functional connectivity* including dynamical processes operating on the network structure, where the graph describing the network architecture is transformed into a weighted graph.

2.1. Structural connectivity

The structural connectivity was investigated by modeling the self-assembled nanowire complex network assuming the NWs as 1D objects randomly distributed and oriented on a 2D plane. The length of the simulated NWs was specified from a normal distribution with mean value of 40 μm and standard deviation of 14 μm, according to the Ag NW length distribution observed experimentally (Supplementary Information S1). An example of a simulated NW network with 1500 NWs randomly dispersed on a 500 $\times$ 500 μm^2 plane is reported in Fig. 1d, where each red dot corresponds to a NW, and each blue dot represents a junction in between intersecting NWs. In order to represent the network as a mathematical object, the NW network was mapped as an undirect graph where each NW represents a fundamental unit (node), while NW junctions are represented by links in between nodes (edges) (Loeffler et al., 2020). Similarly, a structural analysis of nanoscale network materials through a graph-theoretical approach has been reported by Vecchio, Mahler, Hammig, and Kotov (2021). The NW network can be represented as a graph $G = (V, E)$, where V and E are the set of nodes and edges, respectively. The graph connectivity is described by the corresponding adjacency matrix that indicates if pairs of nodes are adjacent or not (Supplementary Information S2). The graph representation of the NW network of Fig. 1d is reported in Fig. 1e where nodes are spatially located on a 2D plane according to the spatial distribution of the NWs. A more abstract representation of the network is depicted in Fig. 1f in terms of a force-directed graph drawing technique obtained with the Kamada & Kawai algorithm (Kamada & Kawai, 1989).

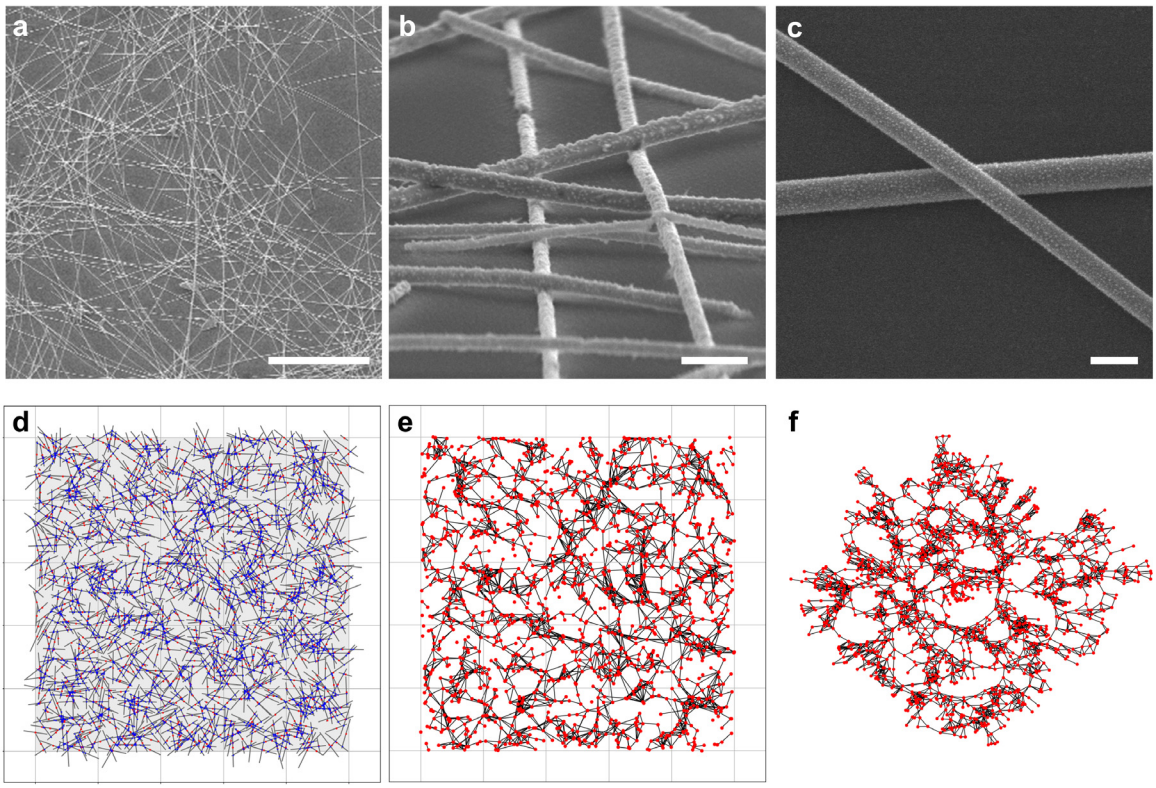

Fig. 1. FE-SEM images and graph representation of self-organized NW networks. a. Top view of an Ag NW network (scale bar, 20 μm), b. tilted view showing a detail of nanoscale cross-point junctions in between intersecting NWs (scale bar, 500 nm) and c. a detail of a single cross-point junction (scale bar, 200 nm). d. Modeling of a network (1500 NWs) on a 500 × 500 μm^2 area (gray area) where red dots represent NWs midpoints, while blue dots represent cross-point junctions at the NWs intersection and e. corresponding graph representation. The grid size is 100 μm. f. Force-directed graph representation according to the Kamada & Kawai algorithm. . (For interpretation of the references to color in this figure legend, the reader is referred to the web version of this article.)

2.1.1. Graph representation and geometric considerations

The structural connectivity of the network strongly depends on the NW density, as can be observed from Fig. 2a,b and c, where a graph representation of NW networks with different normalized densities of NW nodes D is reported (corresponding network models and force-directed graph representations are reported in Supplementary Information S3). The normalized density of nodes D was calculated as $D = N\frac{\langle L\rangle^2}{S^2}$, where N is the number of NW nodes, $\langle L\rangle$ is the average NW length and S is the size of the 2D region where the NWs are randomly deposited (Forró, Demkó, Weydert, Vörös, & Tybrandt, 2018). As expected, increasing the density of NW nodes results in an increasing probability of nanowire overlapping to form NW junction edges with increased network complexity. This aspect can be quantified by considering the node degree (k), i.e. the number of connections that a node establishes with other nodes, and the corresponding degree distribution representing the probability distribution of node degrees (p_k) over the whole network. The degree of nodes distribution corresponding to graphs in Fig. 2a–c is reported in Fig. 2d–f, respectively. While in case of low density of nodes ($D = 1.9$) the most prominent degree of nodes is 0, meaning that most of the NWs are isolated, an asymmetric distribution of nodes was observed to shift towards higher values of k by increasing the NW density. The degree of nodes distribution of the NW network was compared with distributions obtained by dispersing NWs drawn with identical length of 40 μm and from a normal distribution with same mean value but with higher standard deviation (std. dev. = 28 μm). As can be observed, a broadening of the NW length distribution resulted in a flattening of the degree of nodes distributions in the corresponding NW network. The degree of nodes distributions tends to a Poisson distribution by narrowing the NW length distribution, as reported in Supplementary Information S4. These results are in agreement with the Poissonian process (or complete spatial randomness process) expected to regulate the number of junctions of 1D objects dispersed on a 2D plane (Heitz, Leroy, Hébrard, & Lallement, 2011). In case of NWs drawn from a normal distribution of lengths, a correlation in between the degree of NW nodes and the NW length can be observed, as reported in Fig. 2h, reflecting the higher probability of longer NWs to form junction edges with neighbor NW nodes. Interestingly, the average degree of nodes $\langle k\rangle$ scales linearly as a function of the normalized network density D, as reported in Fig. 2i. The average degree of nodes $\langle k\rangle$ is described by the relationship:

$$\langle k\rangle = P \cdot \pi D \tag{1}$$

where $P = (0.195 \pm 0.001)$ is extracted from the linear fit. Interestingly, the value of P obtained in the framework of a graph theory approach is in agreement with the theoretical mean contact probability value $P_{cont} = 0.2027$ expected from geometrical considerations in case of intersecting 1D objects, irrespective of the network density (Heitz et al., 2011). In this framework, the average density of junction edges for unit area is expressed as:

$$j = \frac{1}{2}n\langle k\rangle \tag{2}$$

where n is the density of NW nodes and $\langle k\rangle$ the average degree of nodes. The constant 1/2 is inserted to avoid double counting of junction edges. By substituting Eq. (1) in Eq. (2), we obtain:

$$j = \frac{1}{2}P \cdot n\pi D \tag{3}$$

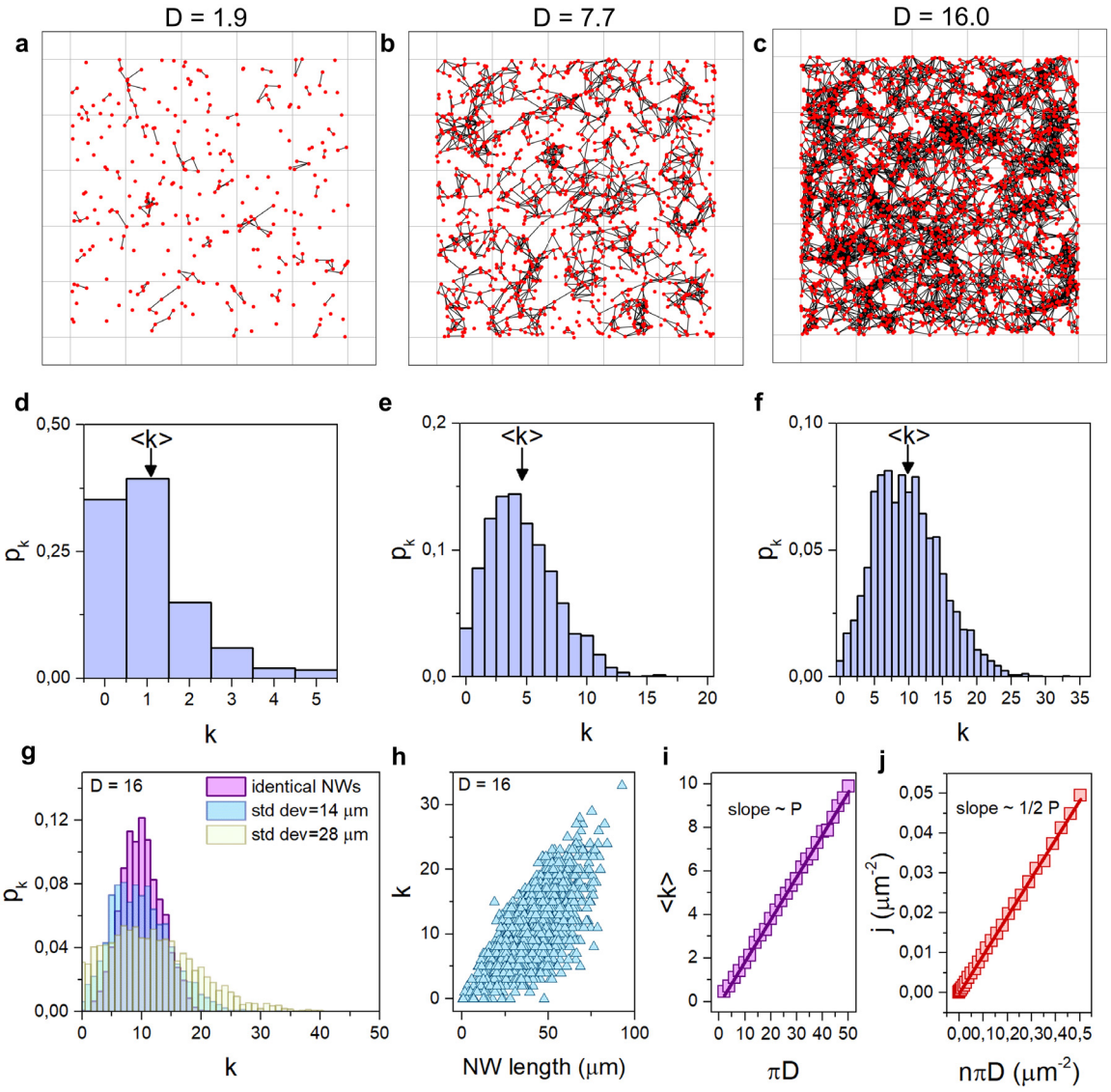

Fig. 2. Graph representation of NW networks with different NW densities. Graphs representation of modeled NW networks with normalized densities of a. $D = 1.9$, b. $D = 7.7$ and c. $D = 16.0$ obtained by randomly dispersing 300, 1200 and 2500 NWs, respectively, on a 500 × 500 μm^2 plane (grid size, 100 μm) and d–f. corresponding degree of nodes k probability distributions. The NW length was drawn according to a normal distribution with mean value of 40 μm and standard deviation of 14 μm according to experimental observations. g. Comparison of the degree of node distribution of a NW network graph with $D = 16.0$ obtained by dispersing NWs with identical length of 40 μm and from a normal distribution with higher standard deviation of 28 μm. h. Correlation of NW node length and node degree corresponding to the network graph in panel c. Relationship in between i. average degree of nodes $\langle k \rangle$ and normalized NW node density D and j. junction density and normalized NW node density D in accordance to Eqs. (1) and (3), respectively.

According to Eq. (3), the junction density j follows a linear relationship with $n\pi D$, with slope of (0.097 ± 0.001) corresponding to $\sim 1/2P$. Note that this relationship implies a quadratic expression between j and n due to the dependence of D on the density of NW nodes and that Eqs. (1) and (3) are valid in case of identical NWs as well as in case of NWs with length drawn according to a normal distribution (Supplementary Information S5). Irrespective of the node density, the adjacent matrices describing NW network graphs are sparse, with sparsity >99.3% (Supplementary Information S6).

2.1.2. Percolation

As a topological invariant of a graph, the number of connected components represents an important feature related to its connectivity. A connected component is a subgraph in which a path connecting each of its nodes exists. As can be observed from Fig. 3a, by increasing the normalized NW density on a 500 × 500 μm^2 plane, the number of components increases for D lower than ∼2.5, while a monotonic decrease is observed for higher values. While for D lower than ∼2.5 an increase of the NW density leads to an emergence of an increasing number of connected components as a consequence of the increased number of junctions, for $D >$ ∼2.5 an increase of NW density is responsible for a progressive coalescence of connected components to form larger connected components. Also, a progressive reduction of the fraction of isolated nodes N_I/N was observed by increasing D due to the increase of the junction probability, as reported in Fig. 3b. Importantly, an analysis of the largest component size revealed the emergence of a giant component by increasing D, as can be observed from Fig. 3c, where the fraction of nodes in the largest component N_{LC}/N is reported as a function of D. Interestingly, an abrupt transition of N_{LC}/N was observed in correspondence with the critical value $D_c \sim 5$, where the probability of a node to be in the largest component corresponds to $\sim 1/2$. By increasing the D value beyond this threshold value, most of the network nodes connect to the largest component and $N_{LC}/N \rightarrow 1$. According

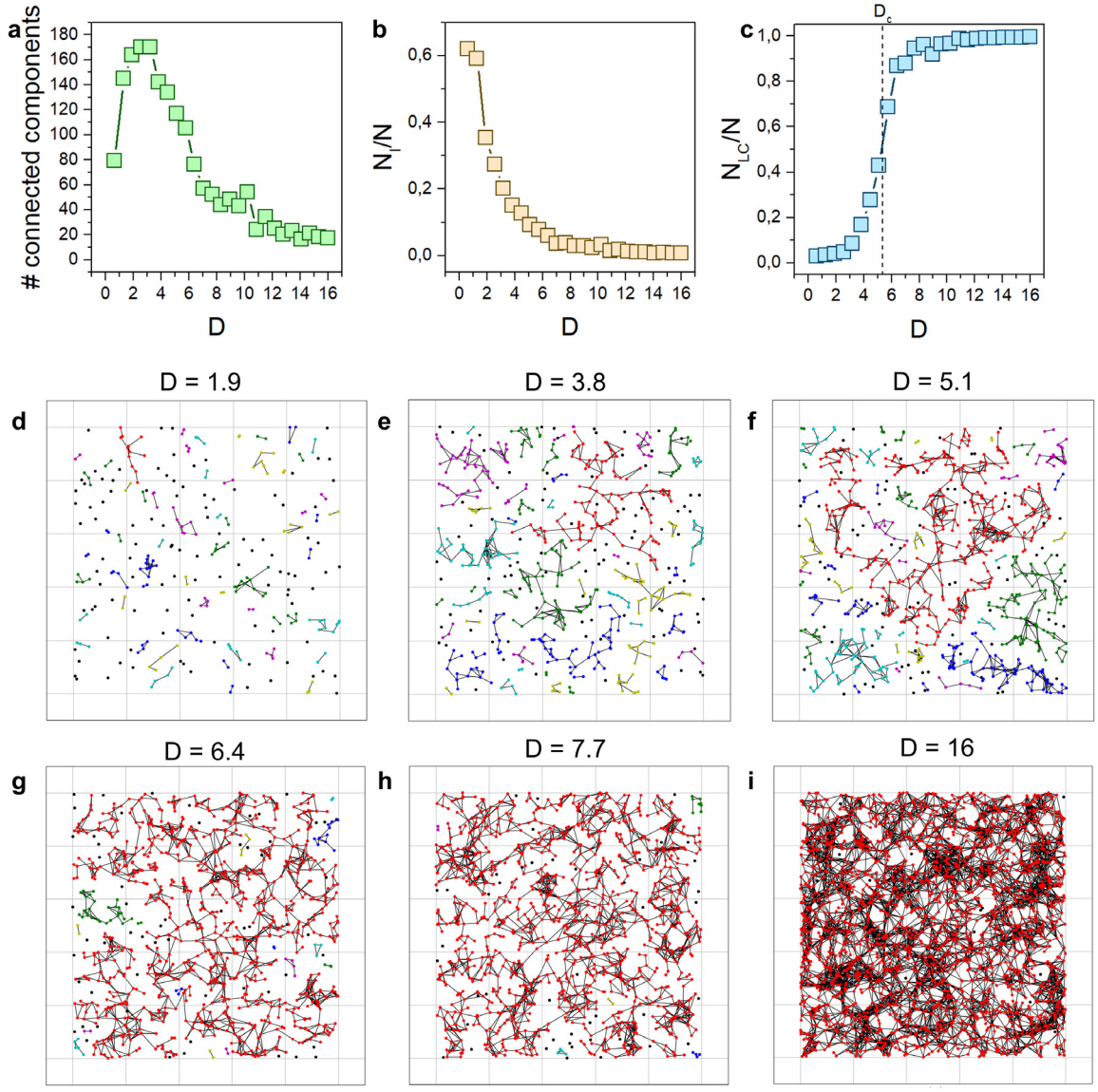

Fig. 3. Emergence of a giant connected component. a. Number of connected components as a function of the NW network normalized density. b. Fraction of isolated nodes as a function of the normalized network density. c. Fraction of nodes in the largest connected components as a function of the normalized network density, showing a phase transition at a critical percolation density of $D_c \sim 5$. d–i. Graph representation of modeled NW networks with increasing densities, showing the emergence of a giant component by increasing D. Nodes belonging to the largest component are depicted in red. . (For interpretation of the references to color in this figure legend, the reader is referred to the web version of this article.)

to percolation theory, this represents a phase transition process from a subcritical regime characterized by a low density of edges and a high number of small components to a supercritical regime where most of the nodes are joined together in a single emerging giant connected component. This aspect is particularly important for the network capacity to transmit information because the emergence of a giant connected component is related to the onset of percolation, since the critical density in NW networks represent the minimal density at which the sample is conductive across the entire plane. Note that the asymptotic critical percolation density value of two-dimensional networks of identical sticks is $D_{C,S\to\infty} = 5.6372858(6)$ (Mietta, Negri, & Tamborenea, 2014), while in real systems this value depends on both the finite system size S and the stick length distribution (Tarasevich & Eserkepov, 2018). The emergence of a giant connected component in the NW network graph by increasing D can be directly visualized in Fig. 3 d–f, where the nodes composing the largest component N_{LC} are depicted in red.

2.1.3. Small-worldness

By analyzing the largest component of the graph, a measure of structure and efficiency of information transport on a network topology is represented by the average shortest path length $\langle L\rangle$, i.e. the shortest path length averaged over all possible pairs of network nodes. The average shortest path length of the largest connected component as a function of the fraction of nodes in the largest component is reported in Fig. 4a. As can be observed, the average shortest path length increases in the subcritical regime for $N_{LC}/N < 1/2$. In the subcritical regime, an increase of the fraction of nodes in the largest component related to an increase of NW density is associated with the progressive increase of the size of the largest connected component that progressively includes spatially distant nodes. After the emergence of the supercritical regime for $N_{LC} > 1/2$, it is interesting to observe that the increase of the largest component size leads to a decrease of the average shortest path length. This is because after the onset of percolation an increase of the NW density results in an increase of the network connectivity with the consequent

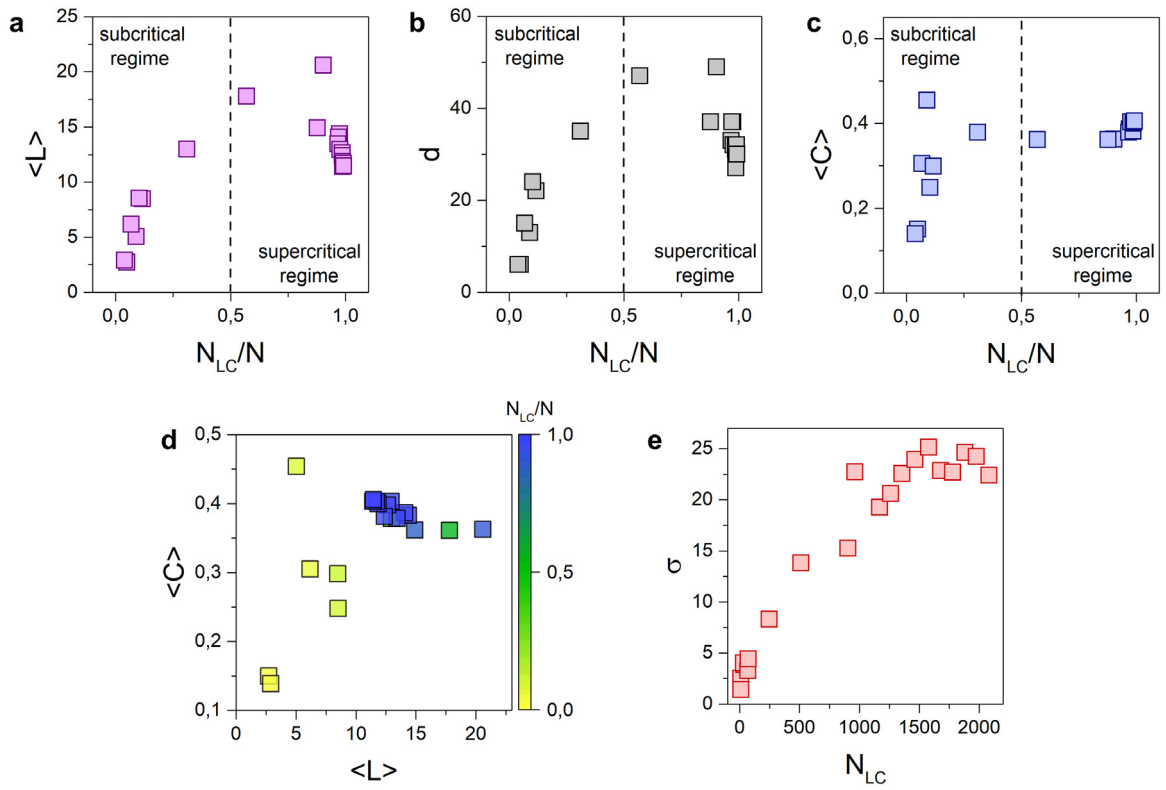

Fig. 4. Analysis of the largest connected component. a. Average shortest path length $\langle L \rangle$, b. diameter D and c. average clustering coefficient as a function of the largest component size N_{LC}/N. Dashed lines represent the percolation threshold. d. Watts–Strogatz cartographic plane showing the average clustering coefficient against the average path length. e. Small-world coefficient as a function of the largest component size N_{LC}.

shortening of distances (path length) in between nodes. Similarly, an increase in the subcritical regime and an increase in the supercritical regime were observed in the largest component diameter d, i.e. the maximum shortest path length in between pair of nodes in the graph, as reported in Fig. 4b. The overall level of clustering coefficient was evaluated by considering the average of the local clustering coefficients $\langle C \rangle$ of the largest component of the graph that, as reported in Fig. 4c, tends to ∼0.4 for $N_{LC}/N \rightarrow 1$. Similar considerations can be drawn by considering the alternative representation of data in the Watts–Strogatz cartographic plane reported in Fig. 4d showing the relationship in between the average path length $\langle L \rangle$ and the average of the local clustering coefficients $\langle C \rangle$. In this framework, it is important to point out that the graph is characterized by a small world architecture (Watts & Strogatz, 1998) if it is characterized by a high degree of clustering and small average path length. Even if the definition of small world networks is still under debate, a quantitative measure of the small-world property is represented by the small-world coefficient (Humphries & Gurney, 2008) defined as $\sigma = \frac{\langle C \rangle}{C_r} / \frac{\langle L \rangle}{L_r}$, where C_r and L_r are the average clustering coefficient and average shortest path length of an equivalent random graph. If $\sigma > 1$ the network exhibits small-word connectivity (Humphries & Gurney, 2008). As can be observed in Fig. 4e, the NW network is small-world since σ is higher than 1, while σ is observed to increase as the size of the largest component increases. In this context, it is worth noticing that the small world character of NW networks can be reduced by stacking of NWs in non-perfect 2D NW networks (Daniels & Brown, 2021).

2.2. Functional connectivity

2.2.1. Graph representation as an electrical circuit

The theory of graphs has been exploited for describing a wide range of electrical networks, from integrated circuits to continent-scale power systems (Dorfler, Simpson-Porco, & Bullo, 2018). Also, a complex network approach can be exploited for modeling carrier transport processes in nanostructure assemblies (Kim & Nam, 2021; Yao, Hsieh, Kong, & Hofmann, 2020). In our case, the propagation of an electrical signal through the network can be investigated by mapping the NW network as an electrical circuit, where the signal transmits through the connected component of a weighted graph. In the approximation of $R_{\text{junction}} \gg R_{\text{wire}}$, as experimentally observed in case of Ag NW networks (Milano, Pedretti et al., 2020), each edge weight corresponds to the resistance of a NW junction. Fig. 5a shows an example of a NW network graph where the electrical signal applied in between source and ground nodes propagates through connected nodes (in blue), while non-connected nodes (in gray) can be disregarded in the electrical circuital description of the problem. The electrical response of the connected component of the network under electrical stimulation can be described by means of the Laplacian matrix L defined as:

$$L = D - W \tag{4}$$

where W is the weighted adjacency matrix and D the degree matrix. Under electrical stimulation, voltage and current Kirchhoff's laws can be solved through the voltage node analysis that corresponds to solving the equation $L^{\dagger}V = I$, where $L^{\dagger}$ is the expanded Laplacian (Zhu et al., 2021), V is the vector of voltages of the graph nodes, while I is the vector of currents flowing into the graph edges. Note that, under electrical stimulation, the network can be also represented as a weighted directed graph where the edge direction represents the current flow direction. Fig. 5b shows a direct visualization of the potential distribution in the graph's nodes reported in Fig. 5a when a voltage ΔV is applied across the selected nodes. As can be observed from the histogram of nodes potentials in Fig. 5c, the vast majority of nodes share

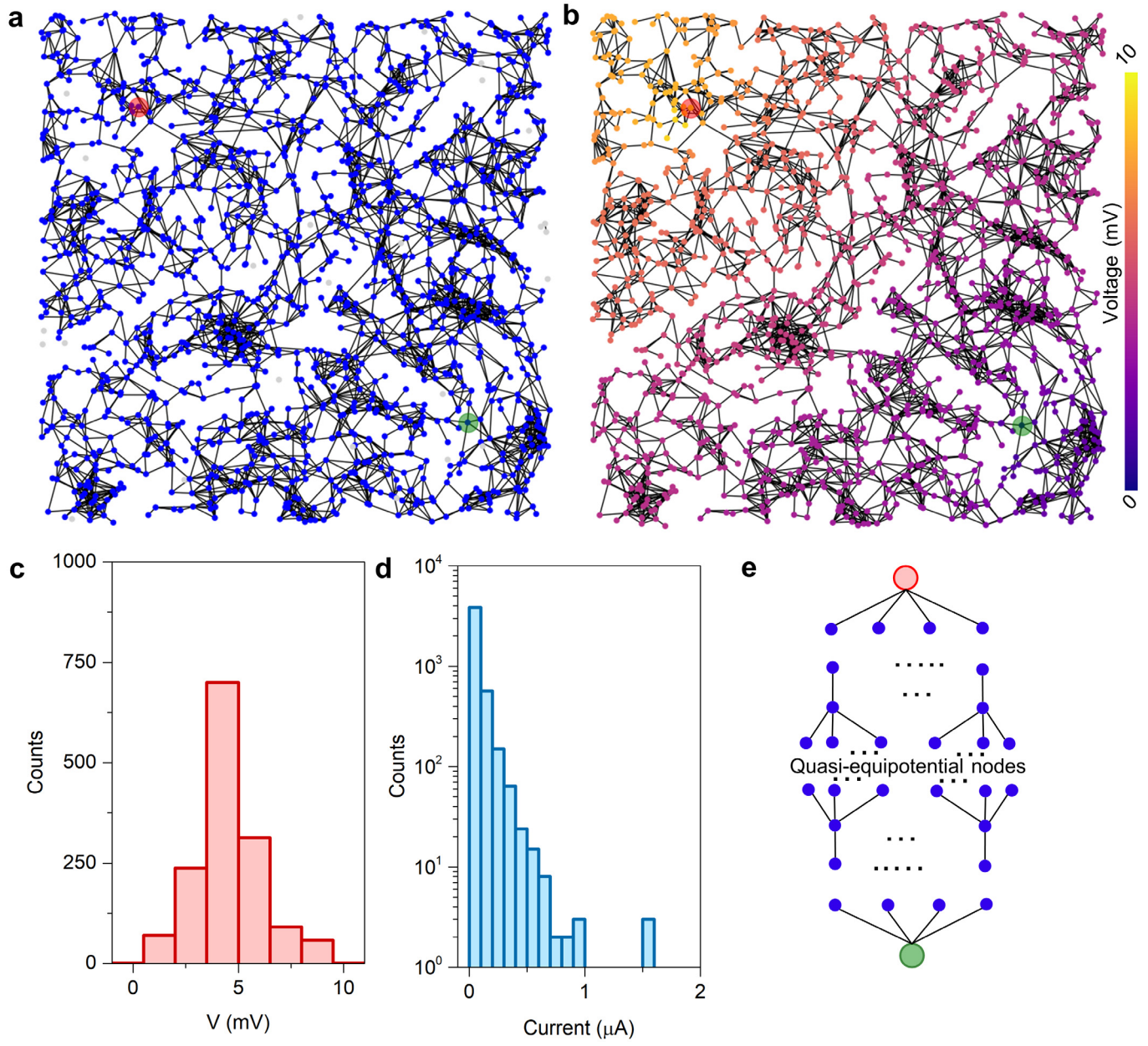

Fig. 5. NW network graph as an electrical circuit. a. Electrical circuit graph representation of a NW network with $D = 9.6$, obtained by randomly dispersing 1500 NW drawn according to a normal distribution with mean value of 40 μm and standard deviation of 14 μm on a 500 × 500 μm^2 plane. Selected nodes of the network where a voltage difference is applied are marked as red (upper left) and black (lower right) circles, representing source and ground nodes, respectively. Only nodes that are connected to source and ground nodes (blue nodes) participate in the propagation of electrical signals, while other nodes (gray nodes) are not involved in the electrical representation of the system. b. Visualization of the potential distribution across nodes of the graph reported in panel a when a voltage difference of 10 mV is applied in between source and ground nodes. Corresponding c. histogram of node potentials and d. histogram of edges currents. Voltage and currents were measured by applying 10 mV in between source and ground nodes, while considering edge resistances of 1 kΩ. d. Schematic representation of the two-sided arborescent structure that emerges when a voltage difference is applied in between two network nodes, where source and ground branches are connected to a quasi-equipotential cluster. . (For interpretation of the references to color in this figure legend, the reader is referred to the web version of this article.)

similar potential forming a large quasi-equipotential cluster. In addition, small currents are observed to flow in the vast majority of edges, as reported in Fig. 5d. As discussed by Kang et al. (2019), this behavior is related to the emergence of a two-sided arborescent structure where the source and ground branches are connected to the quasi-equipotential cluster as schematized in Fig. 4e. In this conduction backbone scheme, the injected current is progressively divided into a large number of smaller current branches at each branching point. Notice that the peak observed in the histogram of Fig. 5c is merely a consequence of the quasi-equipotential cluster discussed above. As the current flows deep into the network, the larger number of connections makes the potential to stabilize its drop (the current lines are less confined causing a reduction of the overall resistance). In addition, because of the harmonic nature of the voltage distribution in a dense Poissonian network, the central peak nearly coincides with the average value $\Delta V/2$.

In this regard, by considering the NW graph as an electrical circuit in static conditions, the distance in between two nodes can be represented by the *resistance distance* metric proposed by Klein and Randić (1993), which takes into account, besides the path length, the existence of multiple paths between nodes that reduce the distance and the redundancy of pathways that provides different routes connecting nodes. The resistance distance, that

diverges from classical geodesic metrics, notably matches with the information distance (Bozzo & Franceschet, 2013). Moreover, the resistance distance in between two network nodes corresponds to the effective resistance in between these nodes, i.e. the physical observable that can be measured by electrically driving the network.

2.2.2. Memristive graph representation and memristive distance

In analogy to the definition of resistance distance, we propose the concept of *"memristive distance"* in graphs where edges can be represented by circuit elements termed "memristors" (from the contraction of "memory" and "resistor") (Chua, 1971) or, more generally, by the class of nonlinear dynamical systems termed "memristive devices and systems" (Chua & Kang, 1976). In these terms, we can define *"memristive graphs"* as a class of graphs where the interaction in between nodes is characterized by nonlinear dynamics. Note that a connection between graph theory and dynamics of memristive circuits have been introduced also by Zegarac and Caravelli (2019). In this context, the nonlinear interactions in between nodes endow memristive graphs with non-trivial and emergent dynamics.

The here proposed definition of "*memristive graphs*" holds in case of NW network graphs where the dynamical behavior of NW junction edges is regulated by its nonlinear memristive behavior. As reported in our previous work (Milano, Pedretti et al., 2020), the memristive junction dynamics are regulated by electrochemical processes at the nanoscale that are responsible for resistive switching through the formation of an Ag conductive bridge across the insulating Polyvinylpyrrolidone (PVP) shell layer connecting the two Ag inner cores (Fig. 6a). A typical experimental switching characteristic of a single junction is reported in Supplementary S7. In this framework, each edge conductance weight G_{ij} in between the intersecting ith and jth NW nodes depends on the history of applied electrical stimulation (Fig. 6b). The nonlinear memristive behavior of each NW junction edge is characterized by short-term synaptic plasticity effects related to the spontaneous relaxation of the junction conductance to the ground state after electrical stimulation due to the spontaneous dissolution of the Ag conductive filament (Milano, Pedretti et al., 2020). The spontaneous dissolution of the Ag filament in NW junctions is driven by the nanobattery effects including minimization of the interfacial energy and internal electromotive forces (Milano et al., 2018; Valov et al., 2013; Wang et al., 2019). These dynamics can be modeled by means of one equation for the electron transport and one equation for the memory state of the memristive edge element. In case of electron transport a linear conduction is assumed, while a voltage-controlled potentiation–depression rate balance equation is exploited for modeling the memory state dynamics (Miranda, Milano, & Ricciardi, 2020). This modeling approach provides a linear differential equation for the memory state with an analytic solution through an implementable recursive method, as described in the following. The current I_{ij} flowing across the intersection in between the ith and jth NW under the action of a voltage difference of ΔV_{ij} can be described by the relation:

$$I_{ij} = \left[G_{\min,\ ij}\left(1 - g_{ij}\right) + G_{\max,\ ij} g_{ij}\right] \Delta V_{ij} \tag{5}$$

where g_{ij} is the normalized conductance (memory state) that assume values in between 0 and 1, while $G_{\min,ij}$ and $G_{\max,ij}$ are the minimum and maximum conductances of the memristive edge ij, respectively. The memory state equation describing short-term plasticity of the edge ij can be expressed by the balance equation (Miranda et al., 2020):

$$\frac{dg_{ij}}{dt} = \kappa_{P,ij}\left(1 - g_{ij}\right) - \kappa_{D,ij} g_{ij} \tag{6}$$

where $\kappa_{P,ij}$ and $\kappa_{D,ij}$ are the potentiation and depression rate coefficients that are assumed to be function of the applied voltage through exponential relationships, as expected for back and forward diffusion of ions:

$$\kappa_{P,ij}(V_{ij}) = \kappa_{P0} exp\left(+\eta_P V_{ij}\right) \tag{7}$$

$$\kappa_{D,ij}(V_{ij}) = \kappa_{D0} exp\left(-\eta_D V_{ij}\right) \tag{8}$$

where $\kappa_{P0}, \kappa_{D0} > 0$ are constants and $\eta_P, \eta_D > 0$ transition rates. Eq. (7) can be recursively solved as (assuming a simulation timestep $\Delta t > 0$) (Miranda et al., 2020):

$$g_{ij,t} = \frac{\kappa_{P,ij}}{\kappa_{P,ij} + \kappa_{D,ij}}\left[1 - e^{-\left(\kappa_{P,ij} + \kappa_{D,ij}\right)\Delta t}\right] + g_{ij,t-1} e^{-\left(\kappa_{P,ij} + \kappa_{D,ij}\right)\Delta t} \tag{9}$$

where $g_{ij,t}$ and $g_{ij,t-1}$ are normalized conductances at times t and $t-1$ of memristive edge ij. Note that Eq. (9), which regulates the nonlinear junction dynamics, is not expressed as a continuous function of t so that it allows to simulate the response of a memristive edge for an arbitrary input voltage (including voltage pulses). Eq. (9) is expressed as the sum of two terms, the first one linked to contribution to the evolution towards the stationary state of the system reached in the long term, and a second term linked to the memory state of the system (hysteresis).

While Fig. 6c shows the experimental time-trace of the effective conductance of an Ag NW network under voltage pulse stimulation in two-terminal configuration, Fig. 6d reports an example of the modeled time-trace of the effective conductance obtained by computing the inverse of the memristive distance in between source and ground nodes of the memristive graph reported in Fig. 5a. In this case, the dynamic behavior of each edge is regulated by the potentiation–depression rate balance equation. For simplicity, the edge-to-edge variability of the memristive response reflecting the junction-to-junction switching variability was neglected, and the dynamic response of each edge was determined by model parameters reported in Supplementary Information S8. As can be observed, the memristive graph modeling is able to capture the main features of the experimental curve with a potentiation of the effective conductance under external stimulation with a voltage pulse, followed by spontaneous relaxation. Also, the model allows direct investigation of the dynamical emergent behavior of the network, as reported in Fig. 6e where the edge conductivities and voltage distributions across the graph over time are reported (Supplementary Movie 1). As a consequence of stimulation, an activation pattern was observed to emerge. Before stimulation (timestep 1), all the network edges were in the low conductance state and the voltage drop across the network is distributed across the graph nodes, as in the static case discussed before. In the first part of voltage pulse stimulation (timestep 2), main changes can be observed in edges near to the source and ground branches of the arborescent structure (i.e. where larger voltage drops in neighbor nodes are present), while less relevant changes can be observed in edges connecting nodes belonging to the quasi-equipotential cluster. Then, the dynamic evolution of the edge conductance is responsible for a progressive redistribution of voltages across graph nodes, leading to the formation of a highly conductive pathway spanning the graph and connecting stimulated nodes (timestep 3). The formation of a conductive pathway connecting stimulating electrodes is in accordance with experimental evidences by lock-in thermography reported by Li et al. (2020) and with computational models reported by Manning et al. (2018) showing the emergence of a conductive pathway in response to current source. After the end of stimulation, the conductance of graph edges tends to restore the initial ground state, resulting in a progressive dissolution of the previously formed conductive pathway (timesteps 4 and 5). Note that, differently from the computational model proposed by

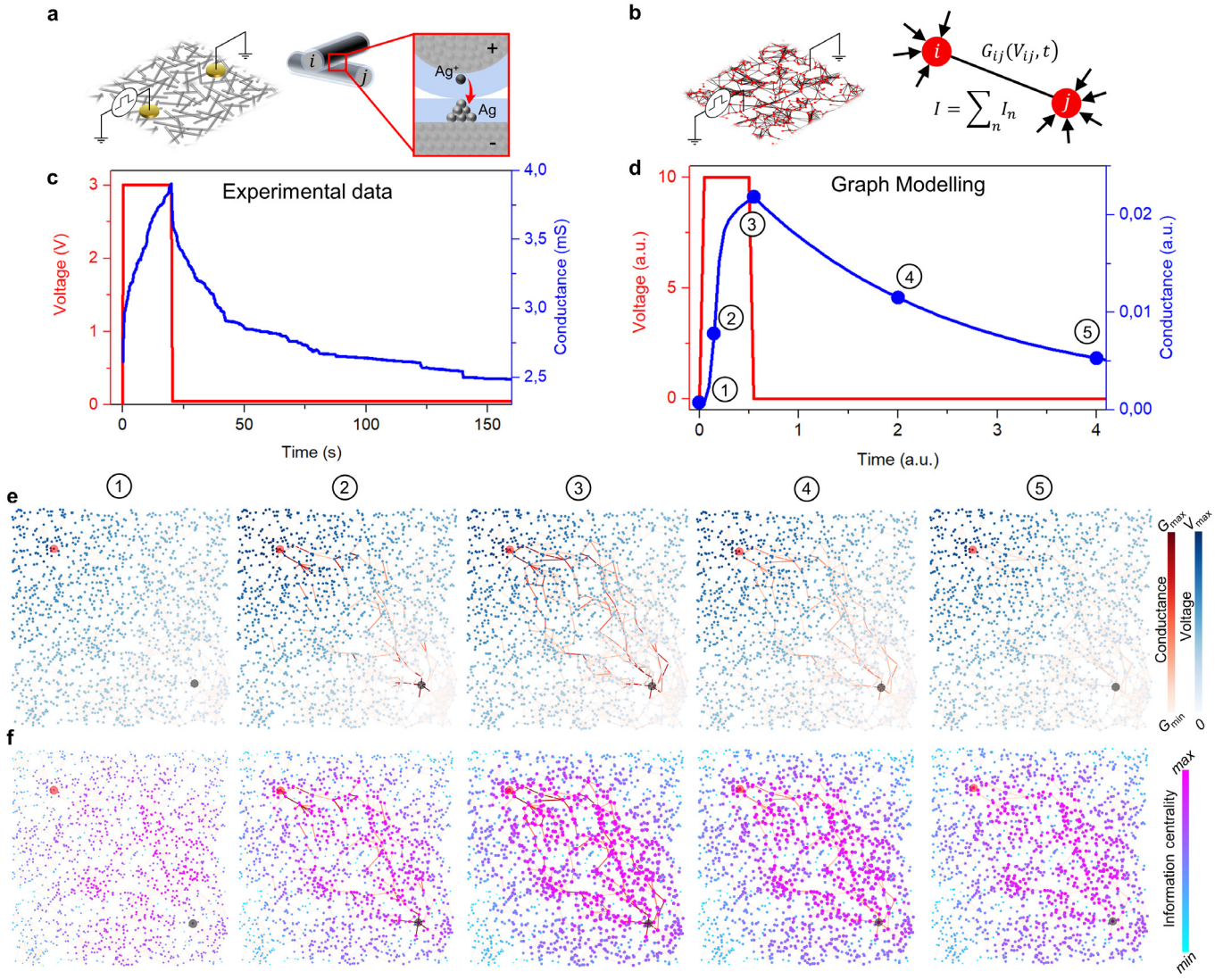

Fig. 6. Emergent memristive behavior of the network. a. Schematic representation of the memristive NW network in two-terminal configuration and schematization of the resistive switching mechanism occurring at NW junctions, where the memristive behavior is regulated by formation/rupture of an Ag conductive filament across the PVP insulating layer bridging the two Ag NW inner cores. Corresponding b. conceptualization of a memristive graph stimulated in between two nodes where the conductance G_{ij} of the edge connecting nodes i and j is regulated by nonlinear dynamics and depends on the history of applied electrical stimulation. c. Experimental temporal evolution of the effective conductance of an Ag NW network under voltage pulse stimulation in two-terminal configuration. d. Evolution of the effective conductance (inverse of the memristive distance) in the graph reported in Fig. 5 while stimulated in between source and ground nodes, where the dynamic behavior of each edge is regulated by the potentiation–depression rate balance equation and e. corresponding representation of the NW graph electrical circuit as a weighted graph where the weight of each edge is represented by the edge red color intensity. The blue node color intensity is proportional to the voltage node while source and ground nodes during stimulation are circled in red and black, respectively. f. Evolution of the information centrality of nodes of the graph during stimulation. While the node color is normalized on the largest value of the corresponding timestep, the node size is proportional to the information centrality value normalized on the larger value obtained during the whole stimulation. As in panel e, the edge color is proportional to the edge conductance. . (For interpretation of the references to color in this figure legend, the reader is referred to the web version of this article.)

Manning et al. (2018), the here proposed model allows to investigate the evolution over time including formation and dissolution of the conductive pathway connecting stimulated nodes.

By considering the notion of memristive distance, it is possible to observe the dynamic evolution of the information centrality (Stephenson & Zelen, 1989), also known as the current-flow closeness centrality (Bozzo & Franceschet, 2013), of the nodes of the memristive graph under external stimulation. This metric is a generalization of centrality, a metric that identify the most influential nodes within a graph, that takes into account also of the enhancement of communication through the network when more routes are possible as in case of the NW network where source and ground nodes can be connected by multiple current pathways. Fig. 6f shows the dynamic evolution of node information centrality in the memristive graph (Supplementary Movie 2). As can be observed, nodes that are located in correspondence of areas where the conductive pathway is formed progressively increase their information centrality in virtue of their increasing influence over the information (current) flow. Note that these are the nodes that, if removed, causes a higher decrease of the transmission network capability (i.e. a higher increase of the network effective resistance). These results show that the emergent behavior of the memristive graph under stimulation results in the formation of a self-selected conductive pathway that maximizes the information flow and minimizes the information distance. It is worth also to highlight that in case of homogeneous and high-density networks where $D \gg D_c$, the network can be approximated as a continuous memristive medium. Therefore, the emergent behavior can be modeled also by means of a regular grid-graph network, where each edge represents the dynamic

behavior of a network area rather that of a single NW junctions (Montano, Milano, & Ricciardi, 2022).

3. Discussion

The interplay in between structure and functions has a crucial role in brain functionalities such as cognition and adaptive behavior, where the connection pattern of neural circuits forms a complex network whose performances are related to its topology (Suárez et al., 2021). Even if it is still unknown how computation and effectiveness emerge from our brain network complexity, it is reasonable to argue that biological neuronal circuits have been optimized through evolution to maximize the computing power and adaptability by continuous refinement of network architecture and wiring diagrams. Similarly, the improvement of artificial neural networks and neuromorphic systems performances in terms of power consumption and effectiveness is expected to rely on the optimization of the structure–function relationship of the neuromorphic hardware. In this scenario, graph theory can provide a unified theoretical framework for exploring biological and artificial neural networks.

Our results show that a graph theoretical approach can be exploited for investigating the structure–function relationship in NW networks. In particular, this approach allows the investigation of the nanonetwork structural connectivity, as shown by revealing the link of the graph theoretical approach with geometrical considerations. Furthermore, the interplay in between the network structure and its capacity to transmit information has been shown by analyzing the phase transition process where results have been found to be consistent with percolation theory.

Also, experimental and modeling results show that the emergent dynamics of NW networks can be described by means of *memristive graphs*, a class of graphs where the interaction in between nodes is regulated by nonlinear dynamics of memristive devices. The concept of memristive graphs can be extended as a theoretical abstraction of other types of memristive networks (including also regular crossbar arrays) and, more in general, to all the complex systems with nonlinear dynamic interactions in between network elements. In all these systems, the concept of *memristive distance* can be explored for unraveling the emergent dynamics of the system and its trafficking of the information flow.

Results show the emergence of activation patterns spanning the network with the formation of self-selected conductive pathways that maximize the information flow and minimize the information distance. In this framework, the peculiar activation pattern relies on the structural topology of the network, as well as on the spatial location of the stimulated nodes. Besides the possibility of simultaneously stimulating multiple network nodes, it is worth noticing that the collective memristive state of the graph depends on the temporal sequence of input signals as well as on the short-term plasticity of network edges. As a consequence, memristive nanonetworks endow the capability of spatio-temporal processing multiple input signals that can be exploited for the physical implementation of unconventional computing paradigms such as reservoir computing (Milano et al., 2021; Nakajima, 2020; Tanaka et al., 2019). Besides reservoir computing, memristive networks can be explored for the solution of shortest-path optimization problems and the traveling salesmen problem, by taking into advantage of the analogue parallel dynamics of a multitude of memristive elements (Pershin & Di Ventra, 2013). In this context, the network structure plays a crucial role in determining the computing performances. Indeed, as reported by Loeffler et al. (2021) by analyzing memory capacity and nonlinear transformation as reservoir computing benchmarks, it was shown that, besides small worldness, network modularity also represents a key aspect for simultaneous computing tasks (multitasking capability). In addition, Hochstetter et al. (2021) have shown that collective dynamics related to the network structure can exhibit avalanche criticality with critical-like state, where information processing was found to be optimized at the edge-of-chaos for computationally complex tasks. Notably, avalanches have been observed close to and above the percolation threshold in NW networks as a consequence of resistive switching dynamics of NW junctions (Hochstetter et al., 2021).

In this framework, we envision that hardware-implemented memristive graphs by means of self-organizing memristive nanonetworks can represent suitable platforms not only for the *in materia* implementation of brain-inspired computing paradigms, but they can also provide inputs to neuroscience for unraveling the relationship between computational capacity, adaptability and structure of our brain with a "learning by doing" approach.

4. Conclusions

In conclusion, structural and functional connectivity of self-organized memristive NW networks was investigated through a graph theoretical approach. Graph theory was shown to provide a suitable theoretical framework for investigating topology and functionalities of memristive nanonetworks, where an emerging behavior arises from the interaction in between a multitude of memristive elements. Results suggest that the emergent network-wide memristive dynamics can be exploited for spatio-temporal processing of input signals, in the framework of unconventional computing paradigms and neuromorphic-type data processing. Our findings can pave the way for rational design of memristive artificial neural networks and neuromorphic systems with optimized structure–function relationship inspired by biological neuronal circuits.

5. Methods

NW network fabrication and characterization

Memristive NW networks were fabricated by randomly dispersing Ag NWs with diameter of 115 nm and length of 20–50 μm in isopropyl alcohol suspension (from Sigma-Aldrich) on a SiO_2(1 μm)/Si insulating commercial substrate (Cultrera et al., 2021; Milano et al., 2020; Milano, Pedretti et al., 2020). The network structural topology and the distribution of NW length was assessed by field emission scanning electron microscopy (FE-SEM; Zeiss Merlin). The electrical behavior of the NW networks was experimentally assessed by realizing metallic Au pads separated by ∼7 mm (approximate pad size of 1.2 × 0.3 mm) on the NW network by sputtering and shadow mask. Electrical characterizations of NW networks were performed by using a Keithley 4200 semiconductor device analyser equipped with Pulse Measuring Units (PMUs) and coupled with a SemiProbe probe station.

Memristive graph modeling

NW network simulations were performed by using Python and analyses were performed by using the NetworkX package (Hagberg, Swart, & Schult, 2008). The random dispersion of 1D sticks on a 2D plane was performed according to the algorithm developed by Loeffler et al. (2020). The parameters of the equation exploited for modeling nonlinear dynamics of the graph edges are reported in Supplementary Information S8.

Graph metrics

Average degree of nodes; being k_i the degree of node i (i.e. the number of wires connected to nanowire i), V the subset of nodes and N the number of nodes of the graph, the average degree of nodes is defined as

$$\langle k \rangle = \frac{1}{N} \sum_{i \in V} k_i$$

Average shortest path length; being the $d(i,j)$ the shortest path from node i and node j, V the subset of nodes and N the number of nodes of the graph, the average shortest path is defined as:

$$\langle L\rangle = \sum_{i,j\in V}^{N} \frac{d(i,j)}{N(N-1)}$$

Graph diameter; the graph diameter is defined as the maximum shortest paths between any two nodes of the network, that is the maximum eccentricity of the graph.

Average local clustering coefficient; being V the subset of nodes and N the number of nodes of the graph, the average clustering coefficient is defined as:

$$\langle C\rangle = \frac{1}{N}\sum_{i\in V} c_i$$

where c_i is the clustering coefficient of node i defined as:

$$c_i = \frac{2T(i)}{\deg(i)(\deg(i)-1)}$$

where $T(i)$ is the number of triangles through node i while $\deg(i)$ is the degree of node i.

Information centrality: for a connected graph where V is the subset of nodes and N the number of nodes, the information centrality of node i is defined as:

$$I_i = \frac{N}{\sum_{j\in V}\frac{1}{I_{ij}}}$$

where I_{ij} is the centrality of a path from node i to j. Information centrality is computed according to the algorithm from Brandes and Fleischer (2005). Refer to J. Stephenson and M. Zelen for the original definition of information centrality (Stephenson & Zelen, 1989).

Declaration of competing interest

The authors declare that they have no known competing financial interests or personal relationships that could have appeared to influence the work reported in this paper.

Code availability

The codes used to generate datasets of simulations can be accessed on GitHub (https://github.com/MilanoGianluca/Memristive_Nanowire_Networks_Connectome).

Data availability

The data that support the findings of this study are openly available on Zenodo (https://doi.org/10.5281/zenodo.6322736).

Acknowledgments

Fabrication of memristive nanowire networks was performed at "Nanofacility Piemonte", a facility supported by the "Compagnia di San Paolo" foundation. Part of this work was supported by the European project MEMQuD, code 20FUN06. This project (EMPIR 20FUN06 MEMQuD) has received funding from the EMPIR programme co-financed by the Participating States and from the European Union's Horizon 2020 research and innovation programme.

Funding

This work was supported by the European Metrology Programme for Innovation and Research, Funder ID: 10.13039/100014132, Grant number: EMPIR 20FUN06 MEMQuD.

Appendix A. Supplementary data

Supplementary data includes details on the distribution of NW length, adjacency matrix, networks with different densities, degree of nodes distribution of networks of identical NWs, average degree of nodes and junction density, adjacency matrix sparsity, resistive switching of a single Ag NW junction, parameters for modelling the nonlinear response of graph edges, video of the evolution of network conductivity and video of the evolution of information centrality.

Supplementary material related to this article can be found online at https://doi.org/10.1016/j.neunet.2022.02.022.

References

Akai-Kasaya, Megumi, Takeshima, Yuki, Kan, Shaohua, Nakajima, Kohei, Oya, Takahide, & Asai, Tetsuya (2022). Performance of reservoir computing in a random network of single-walled carbon nanotubes complexed with polyoxometalate. *Neuromorphic Computing and Engineering*, *2*(1), Article 014003.

Bozzo, Enrico, & Franceschet, Massimo (2013). Resistance distance, closeness, and betweenness. *Social Networks*, *35*(3), 460–469.

Brandes, Ulrik, & Fleischer, Daniel (2005). *Lecture notes in computer science*: *vol. 3404, Centrality measures based on current flow* (pp. 533–544).

Christensen, Dennis Valbjørn, Dittmann, Regina, Linares-Barranco, Bernabe, Sebastian, Abu, Le Gallo, Manuel, Redaelli, Andrea, et al. (2022). 2022 Roadmap on neuromorphic computing and engineering. *Neuromorphic Computing and Engineering*, *2*(1), 0–31.

Chua, Leon (1971). Memristor-The missing circuit element. *IEEE Transactions on Circuit Theory*, *18*(5), 507–519.

Chua, L. O., & Kang, Sung Mo (1976). Memristive devices and systems. *Proceedings of the IEEE*, *64*(2), 209–223.

Cultrera, Alessandro, Milano, Gianluca, Leo, Natascia De, Ricciardi, Carlo, Boarino, Luca, & Callegaro, Luca (2021). Recommended implementation of electrical resistance tomography for conductivity mapping of metallic nanowire networks using voltage excitation. *Scientific Reports*, *11*(1), 13167.

Daniels, Ryan K., & Brown, Simon A. (2021). Nanowire networks: How does small-world character evolve with dimensionality? *Nanoscale Horizons*, *6*(6), 482–488.

Diaz-Alvarez, A., Higuchi, R., Li, Q., Shingaya, Y., & Nakayama, T. (2020). Associative routing through neuromorphic nanowire networks. *AIP Advances*, *10*(2), Article 025134.

Diaz-Alvarez, Adrian, Higuchi, Rintaro, Sanz-Leon, Paula, Marcus, Ido, Shingaya, Yoshitaka, Stieg, Adam Z., et al. (2019). Emergent dynamics of neuromorphic nanowire networks. *Scientific Reports*, *9*(1), 14920.

Dorfler, Florian, Simpson-Porco, John W., & Bullo, Francesco (2018). Electrical networks and algebraic graph theory: Models, properties, and applications. *Proceedings of the IEEE*, *106*(5), 977–1005.

Eichelmann, H., Oja, V., Eatherall, A., a Walker, D., & and Biological Sciences (1986). The structure of the nervous system of the nematode caenorhabditis elegans. *Philosophical Transactions of the Royal Society of London. B, Biological Sciences*, *314*(1165), 1–340.

Forró, Csaba, Demkó, László, Weydert, Serge, Vörös, János, & Tybrandt, Klas (2018). Predictive model for the electrical transport within nanowire networks. *ACS Nano*, *12*(11), 11080–11087.

Hagberg, Aric, Swart, Pieter J., & Schult, Daniel A. (2008). Exploring network structure, dynamics, and function using NetworkX. In *Proceedings of the 7th Python in science conference (SciPy2008)*. Pasadena (pp. 11–15).

Heitz, Jérôme, Leroy, Yann, Hébrard, Luc, & Lallement, Christophe (2011). Theoretical characterization of the topology of connected carbon nanotubes in random networks. *Nanotechnology*, *22*(34), Article 345703.

Hochstetter, Joel, Zhu, Ruomin, Loeffler, Alon, Diaz-Alvarez, Adrian, Nakayama, Tomonobu, & Kuncic, Zdenka (2021). Avalanches and edge-of-chaos learning in neuromorphic nanowire networks. *Nature Communications*, *12*(1), 4008.

Humphries, Mark D., & Gurney, Kevin (2008). Network 'Small-World-Ness': A quantitative method for determining canonical network equivalence edited by O. Sporns. *PLoS ONE*, *3*(4), Article e0002051.

Kamada, Tomihisa, & Kawai, Satoru (1989). An algorithm for drawing general undirected graphs. *Information Processing Letters*, *31*(1), 7–15.

Kang, Min-Yeong, Berthelot, Geoffroy, Tupikina, Liubov, Nicolaides, Christos, Colonna, Jean-Francois, Sapoval, Bernard, et al. (2019). Morphological organization of point-to-point transport in complex networks. *Scientific Reports*, *9*(1), 8322.

Kim, Dongjae, & Nam, Jaewook (2021). Analyzing conducting rod networks using centrality. *Electrochimica Acta*, *370*, Article 137725.

Klein, D. J., & Randić, M. (1993). Resistance distance. *Journal of Mathematical Chemistry*, *12*(1), 81–95.

Li, Qiao, Diaz-Alvarez, Adrian, Iguchi, Ryo, Hochstetter, Joel, Loeffler, Alon, Zhu, Ruomin, et al. (2020). Dynamic electrical pathway tuning in neuromorphic nanowire networks. *Advanced Functional Materials*, *2003679*, Article 2003679.

Lilak, Sam, Woods, Walt, Scharnhorst, Kelsey, Dunham, Christopher, Teuscher, Christof, Stieg, Adam Z., et al. (2021). Spoken digit classification by in-materio reservoir computing with neuromorphic atomic switch networks. *Frontiers in Nanotechnology*, *3*(May), 1–11.

Loeffler, Alon, Zhu, Ruomin, Hochstetter, Joel, Diaz-Alvarez, Adrian, Nakayama, Tomonobu, Shine, James M., et al. (2021). Modularity and multitasking in neuro-memristive reservoir networks. *Neuromorphic Computing and Engineering*, *1*(1), Article 014003.

Loeffler, Alon, Zhu, Ruomin, Hochstetter, Joel, Li, Mike, Fu, Kaiwei, Diaz-Alvarez, Adrian, et al. (2020). Topological properties of neuromorphic nanowire networks. *Frontiers in Neuroscience*, *14*(March).

Mallinson, J. B., Shirai, S., Acharya, S. K., Bose, S. K., Galli, E., & Brown, S. A. (2019). Avalanches and criticality in self-organized nanoscale networks. *Science Advances*, *5*(11), eaaw8438.

Manning, Hugh G., Niosi, Fabio, da Rocha, Claudia Gomes, Bellew, Allen T., O'Callaghan, Colin, Biswas, Subhajit, et al. (2018). Emergence of winner-takes-all connectivity paths in random nanowire networks. *Nature Communications*, *9*(1), 3219.

Mietta, J. L., Negri, R. M., & Tamborenea, P. I. (2014). Numerical simulations of stick percolation: Application to the study of structured magnetorheological elastomers. *The Journal of Physical Chemistry C*, *118*(35), 20594–20604.

Milano, Gianluca, Cultrera, Alessandro, Bejtka, Katarzyna, De Leo, Natascia, Callegaro, Luca, Ricciardi, Carlo, et al. (2020). Mapping time-dependent conductivity of metallic nanowire networks by electrical resistance tomography toward transparent conductive materials. *ACS Applied Nano Materials*, acsanm.0c02204.

Milano, Gianluca, Luebben, Michael, Ma, Zheng, Dunin-Borkowski, Rafal, Boarino, Luca, Pirri, Candido F., et al. (2018). Self-limited single nanowire systems combining all-in-one memristive and neuromorphic functionalities. *Nature Communications*, *9*(1), 5151.

Milano, Gianluca, Pedretti, Giacomo, Fretto, Matteo, Boarino, Luca, Benfenati, Fabio, Ielmini, Daniele, et al. (2020). Brain-inspired structural plasticity through reweighting and rewiring in multi-terminal self-organizing memristive nanowire networks. *Advanced Intelligent Systems*, *2*(8), Article 2000096.

Milano, Gianluca, Pedretti, Giacomo, Montano, Kevin, Ricci, Saverio, Hashemkhani, Shahin, Boarino, Luca, et al. (2021). In materia reservoir computing with a fully memristive architecture based on self-organizing nanowire networks. *Nature Materials*.

Milano, Gianluca, Porro, Samuele, Valov, Ilia, & Ricciardi, Carlo (2019). Recent developments and perspectives for memristive devices based on metal oxide nanowires. *Advanced Electronic Materials*, *5*(9), Article 1800909.

Miranda, Enrique, Milano, Gianluca, & Ricciardi, Carlo (2020). Modeling of short-term synaptic plasticity effects in ZnO nanowire-based memristors using a potentiation-depression rate balance equation. *IEEE Transactions on Nanotechnology*, *19*, 609–612.

Montano, Kevin, Milano, Gianluca, & Ricciardi, Carlo (2022). Grid-graph modeling of emergent neuromorphic dynamics and heterosynaptic plasticity in memristive nanonetworks. *Neuromorphic Computing and Engineering*, 0–22.

Nakajima, Kohei (2020). Physical reservoir computing—an introductory perspective. *Japanese Journal of Applied Physics*, *59*(6), Article 060501.

Pantone, Ross D., Kendall, Jack D., & Nino, Juan C. (2018). Memristive nanowires exhibit small-world connectivity. *Neural Networks*, *106*, 144–151.

Pershin, Yuriy V., & Di Ventra, Massimiliano (2013). Self-organization and solution of shortest-path optimization problems with memristive networks. *Physical Review E*, *88*(1), Article 013305.

Pike, Matthew D., Bose, Saurabh K., Mallinson, Joshua B., Acharya, Susant K., Shirai, Shota, Galli, Edoardo, et al. (2020). Atomic scale dynamics drive brain-like avalanches in percolating nanostructured networks. *Nano Letters*, *20*(5), 3935–3942.

Scharnhorst, Kelsey S., Carbajal, Juan P., Aguilera, Renato C., Sandouk, Eric J., Aono, Masakazu, Stieg, Adam Z., et al. (2018). Atomic switch networks as complex adaptive systems. *Japanese Journal of Applied Physics*, *57*(3S2), 03ED02.

Shirai, Shota, Acharya, Susant Kumar, Bose, Saurabh Kumar, Mallinson, Joshua Brian, Galli, Edoardo, Pike, Matthew D., et al. (2020). Long-range temporal correlations in scale-free neuromorphic networks. *Network Neuroscience*, *4*(2), 432–447.

Sporns, Olaf (2011). The human connectome: A complex network. *Annals of the New York Academy of Sciences*, *1224*(1), 109–125.

Sporns, Olaf (2018). Graph theory methods: Applications in brain networks. *Dialogues in Clinical Neuroscience*, *20*(2), 111–121.

Sporns, Olaf, Tononi, Giulio, & Kötter, Rolf (2005). The human connectome: A structural description of the human brain. *PLoS Computational Biology*, *1*(4), Article e42.

Stephenson, Karen, & Zelen, Marvin (1989). Rethinking centrality: Methods and examples. *Social Networks*, *11*(1), 1–37.

Stieg, Adam Z., Avizienis, Audrius V., Sillin, Henry O., Martin-Olmos, Cristina, Lam, Miu-Ling, Aono, Masakazu, et al. (2014). Self-organized atomic switch networks. *Japanese Journal of Applied Physics*, *53*(1S), 01AA02.

Strogatz, Steven H. (2001). Exploring complex networks. *Nature*, *410*(6825), 268–276.

Suarez, Laura E., Kendall, Jack D., & Nino, Juan C. (2018). Evaluation of the computational capabilities of a memristive random network (MN3) under the context of reservoir computing. *Neural Networks*, *106*, 223–236.

Suárez, Laura E., Markello, Ross D., Betzel, Richard F., & Misic, Bratislav (2020). Linking structure and function in macroscale brain networks. *Trends in Cognitive Sciences*, *24*(4), 302–315.

Suárez, Laura E., Richards, Blake A., Lajoie, Guillaume, & Misic, Bratislav (2021). Learning function from structure in neuromorphic networks. *Nature Machine Intelligence*, *3*(9), 771–786.

Tanaka, Hirofumi, Akai-Kasaya, Megumi, TermehYousefi, Amin, Hong, Liu, Fu, Lingxiang, Tamukoh, Hakaru, et al. (2018). A molecular neuromorphic network device consisting of single-walled carbon nanotubes complexed with polyoxometalate. *Nature Communications*, *9*(1), 2693.

Tanaka, Gouhei, Yamane, Toshiyuki, Héroux, Jean Benoit, Nakane, Ryosho, Kanazawa, Naoki, Takeda, Seiji, et al. (2019). Recent advances in physical reservoir computing: A review. *Neural Networks*, *115*, 100–123.

Tang, Jianshi, Yuan, Fang, Shen, Xinke, Wang, Zhongrui, Rao, Mingyi, He, Yuanyuan, et al. (2019). Bridging biological and artificial neural networks with emerging neuromorphic devices: Fundamentals, progress, and challenges. *Advanced Materials*, *31*(49), Article 1902761.

Tarasevich, Yuri Yu, & Eserkepov, Andrei V. (2018). Percolation of sticks: Effect of stick alignment and length dispersity. *Physical Review E*, *98*(6), 1–6.

Turnbull, Laura, Hütt, Marc-Thorsten, Ioannides, Andreas A., Kininmonth, Stuart, Poeppl, Ronald, Tockner, Klement, et al. (2018). Connectivity and complex systems: Learning from a multi-disciplinary perspective. *Applied Network Science*, *3*(1), 11.

Upadhyay, Navnidhi K., Jiang, Hao, Wang, Zhongrui, Asapu, Shiva, Xia, Qiangfei, & Joshua Yang, J. (2019). Emerging memory devices for neuromorphic computing. *Advanced Materials Technologies*, *4*(4), Article 1800589.

Usami, Yuki, Ven, Bram, Mathew, Dilu G., Chen, Tao, Kotooka, Takumi, Kawashima, Yuya, et al. (2021). In-materio reservoir computing in a sulfonated polyaniline network. *Advanced Materials*, *2102688*, Article 2102688.

Valov, I., Linn, E., Tappertzhofen, S., Schmelzer, S., van den Hurk, J., Lentz, F., et al. (2013). Nanobatteries in redox-based resistive switches require extension of memristor theory. *Nature Communications*, *4*(1), 1771.

Vecchio, Drew A., Mahler, Samuel H., Hammig, Mark D., & Kotov, Nicholas A. (2021). Structural analysis of nanoscale network materials using graph theory. *ACS Nano*, *15*(8), 12847–12859.

Vecchio, Fabrizio, Miraglia, Francesca, & Rossini, Paolo Maria (2017). Connectome: Graph theory application in functional brain network architecture. *Clinical Neurophysiology Practice*, *2*, 206–213.

Wang, Wei, Wang, Ming, Ambrosi, Elia, Bricalli, Alessandro, Laudato, Mario, Sun, Zhong, et al. (2019). Surface diffusion-limited lifetime of silver and copper nanofilaments in resistive switching devices. *Nature Communications*, *10*(1), 81.

Watts, Duncan J., & Strogatz, Steven H. (1998). Collective dynamics of 'Small-World' networks. *Nature*, *393*(6684), 440–442.

Witvliet, Daniel, Mulcahy, Ben, Mitchell, James K., Meirovitch, Yaron, Berger, Daniel R., Wu, Yuelong, et al. (2021). Connectomes across development reveal principles of brain maturation. *Nature*, *596*(7871), 257–261.

Xia, Qiangfei, & Yang, J. Joshua (2019). Memristive crossbar arrays for brain-inspired computing. *Nature Materials*, *18*(4), 309–323.

Yao, Heming, Hsieh, Ya-Ping, Kong, Jing, & Hofmann, Mario (2020). Modelling electrical conduction in nanostructure assemblies through complex networks. *Nature Materials*, *19*(7), 745–751.

Zegarac, A., & Caravelli, F. (2019). Memristive networks: From graph theory to statistical physics. *EPL (Europhysics Letters)*, *125*(1), 10001.

Zhu, Ruomin, Hochstetter, Joel, Loeffler, Alon, Diaz-Alvarez, Adrian, Nakayama, Tomonobu, Lizier, Joseph T., et al. (2021). Information dynamics in neuromorphic nanowire networks. *Scientific Reports*, *11*(1), 13047.